Towards stable evolutions of excised black hole spacetimes via the ADM equations: A spherically symmetric test

Luis Lehner,[1] Mijan Huq,[2] Matt Anderson,[1] Erin Bonning,[1] Doug Schaefer,[1] and Richard Matzner[1]
[1]*Center for Relativity, The University of Texas at Austin, Austin, Texas 78712*
[2]*Department of Astronomy & Astrophysics, and Center for Gravitational Physics & Geometry, The Pennsylvania State University, University Park, Pennsylvania 16802*
(Received 16 March 2000; published 25 July 2000)

Within the numerical relativity community, much effort has been devoted to simulate the coalescence of black hole binaries. A key problem in attempting such a simulation is the handling of the singularity present in each hole. A very promising approach to address this issue is the excision of the singularities from the computational domain. However, to date there have been only a few restricted examples in the literature showing that this approach yields long-term stable simulations in 3+1 formulations. It has been argued that the form of the Einstein field equations normally used, namely, the Arnowitt-Deser-Misner (ADM) equations, when applied to black hole excision, could be the cause of instabilities. By means of perturbative and numerical studies in spherical symmetry [one-dimensional (1D)], we show that successful numerical solutions of excised, single black hole spacetimes can be constructed with the ADM formulation of Einstein equations if the appropriate choice of gauge or coordinate conditions is made. Preliminary 3D results are consistent with the 1D studies.

PACS number(s): 04.25.−g, 04.30.−w

I. INTRODUCTION

Since the mid 1970s, variations of the so called Arnowitt-Deser-Misner (ADM) formulation [1] of the Einstein field equations have been the favored system of equations by the numerical relativity community for studies of both cosmological and compact-object spacetimes. In the following, we use ''ADM'' as a generic term referring to the class of 3+1 formulations of Einstein equations that have as fundamental variables tensors related algebraically to the ADM quantities g_{ij} and π^{ij}. Given a foliation of the spacetime, g_{ij} denotes the intrinsic metric of the spacelike hypersurfaces that define the foliation, with π^{ij} the momentum density associated with g_{ij}. Many formulations use, instead of π^{ij}, the extrinsic curvature K_{ij} of the hypersurfaces. In these variables, Einstein equations become first order in time equations for the metric and the extrinsic curvature. For this reason, these systems of equations are called $\dot{g}$-$\dot{K}$ formulations. Throughout this paper, spatial indices are denoted with latin letters, and units are such that $c=G=1$.

With the ADM approach, researchers have been able to study a variety of problems, and interesting physics has been obtained from simulations produced with its numerical implementation. However, at present, we face the most demanding task to date: to simulate a binary black hole merger and obtain the gravitational radiation wave forms produced in such a system. Black hole collision simulations must be done in a fully three-dimensional (3D) setting because of the absence of symmetries; as a consequence, the computational task is formidable in terms of accessible resources. Even situations with special symmetries that are intrinsically 1D, such as the case of a single black hole, have proven to be an incredibly challenging task, requiring much more effort than had been anticipated. Instabilities observed in 3D simulations have raised two distinct types of still open questions.

The choice of ADM-like formulations. That is, what is the impact of the choice of a formulation of Einstein equations on the stability properties of its numerical implementation? For example, would formulations or modifications where the constraints are enforced improve the situation? Would a flux-conservative form aid in the solution of problems with black hole excisions? Would a well posed system be capable of ''removing'' instabilities; would the fact that the solutions to well posed systems cannot grow arbitrarily fast simplify the attainment of a stable implementation of the system?

The choice of gauge conditions. That is, what is the effect of the choice of gauge or coordinate conditions on the onset of instabilities? Are some choices of gauge conditions more convenient in handling black hole excision? Is there indication that successful prescriptions of gauge conditions would be global, or, could a set of gauge conditions, with each condition applied in different sectors of the computational domain, have a better chance of preventing the presence of instabilities?

In response to the first class of questions, in recent years a number of new formulations have been introduced as candidates to model the Einstein equations. These formulations were obtained with different goals in mind, namely, explicit hyperbolicity [2–6], flux conservation [7], separation of modes [6,8–10], etc. Each of these formulations has at least one of these nice features and is therefore enticing. Unfortunately, a common drawback is that they involve more, and in some cases many more, variables than in the standard ADM formulation, thus imposing further demands on computer environments. Furthermore, preliminary implementation of singularity excision in some of these formulations have shown similar problems to those seen in the traditional ADM formulation [11,12].

On the other hand, at first sight the standard ADM formulation would seem to suffer from some disadvantages since it is neither explicitly hyperbolic nor are the equations ex-

pressed in a flux conservative form. Yet, years of experience with this system, which has the minimum set of variables for a $3+1$ formulation, puts at least at present the ADM form of Einstein equations on an equal footing with the others. Furthermore, one should keep in mind that much of the progress obtained by other formalisms has been built on techniques first developed for the ADM system, and hence research in this direction is important for its own merits and for its consequences on newer approaches.

Here, using the standard ADM formulation, we present a detailed study closely related to the class of questions in connection with the choice of gauge. For simplicity, we consider only the spherically symmetric case, both from the analytic and numerical points of view. This 1D study has been motivated by the difficulties, i.e., ''instabilities,''[1] in our application of the ADM formulation to the evolution of single black hole spacetimes in a 3D setting. Single black hole, 3D evolutions are used as a benchmark problem in the development of numerical codes to simulate black hole collisions. The observed instabilities in those 3D simulations could be of numerical origin, for instance, unstable discretization schemes, or they could also be already present at the continuum level. In addition, boundary conditions and gauge conditions could play a fundamental role in the stability properties of the simulation. The possible numerical and continuum sources of instabilities are often coupled and difficult to separate. By considering the problem in 1D, the task of identifying the sources of instabilities becomes more tractable. Of course, in order to obtain better insight applicable to 3D situations, one must try to mimic in the 1D setup what takes places in the full 3D problem. Even then, it is likely that some of the numerical sources of instabilities are dimensional dependent and thus will be missed by the present study. In spherical symmetry there have been a number of papers in the literature that discuss and use excision techniques in black hole evolutions. Seidel and Suen [13] proposed a causal differencing algorithm in a paper that demonstrated black hole excision using a horizon locked coordinate. Marsa and Choptuik [14] use a partially constrained evolution in addition to a gauge choice that imposes horizon-locking also, Scheel *et al.* [15] use causal differencing with a hyperbolic formulation of the $3+1$ equations which requires the addition of constraints to the evolution equations, and lastly Gundlach and Walker [16] demonstrate the use of causal differencing for the Bona-Masso formulation of the Einstein equations.

In particular, causal differencing takes advantage of the fact that the causal domain of dependence of points inside the apparent horizon are tilted away from the singularity. Hence, by deforming the numerical integration stencil, the evolution equations can be integrated without the need of specifying boundary data at inner boundary points. The apparent horizon is that topological two sphere whose outgoing null rays have zero divergence, and, if it exists, it lies inside the event horizon [17].

[1]We explain below our heuristic use of the term ''instability.''

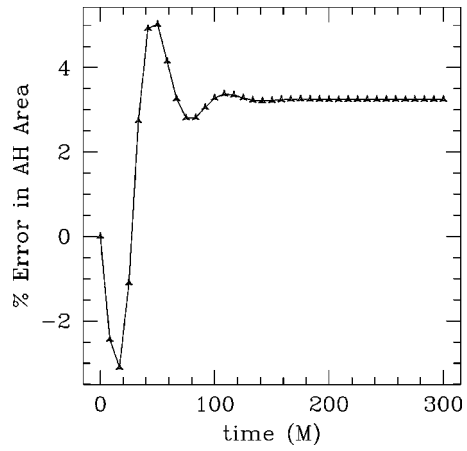

FIG. 1. The percentage error in the area of the apparent horizon is shown for a 3D run with the outer boundary at 3.33 M. This run was stable with the apparent horizon oscillating radially before settling down to about 3% error.

We focus our attention on unconstrained evolutions and to situations where horizon-locking coordinates are implemented such that the algorithms mimic the 3D codes that we use. The basic task at hand is to solve a set of coupled nonlinear time-dependent partial differential equations. In addition we have to pick boundary conditions at the outer boundary of the computational domain, and construct ''stable'' finite difference discretization that respects the causal structure of the spacetime in the vicinity of the excised region. In addition, since after all we are solving Einstein equations, we still have four gauge degrees of freedom to specify through the lapse and shift vector at every time slice. A ''bad'' choice of lapse function and shift vector or a failure to maintain ''gauge conditions'' can lead to coordinate pathologies. Lastly, the Einstein equations in the ADM or $3+1$ form separate into a set of four constraint equations and twelve first order in time evolution equations. In our 3D, and here in our 1D codes, after the initial time we solve only the evolution equations and hence have an *unconstrained evolution*. As a result, constraint violating modes might be present that could lead to a failure of a numerical simulation.

In the 3D results thus far, we have found a peculiar dependence on the placement of outer boundaries on the stability of analytically stationary single-black-hole evolutions. Placing outer boundaries between $3M$ to $4M$, with M the mass of the black hole, can yield stable evolutions in 3D, yet moving the boundaries outwards from $4M$ leads to unbounded growth which has a characteristic time that depends sensitively on the location of the outer boundary. Figure 1 shows the percentage error in the area of the apparent horizon for a stable 3D run with boundaries placed at 3.33M. In this run the apparent horizon oscillates radially before settling. Figure 2 shows the l_∞ norm of the residual of the normalized Hamiltonian constraint as a function of time for various runs in 3D. Note the dependence of stability and maximum runtime on the location of the outer boundary (denoted by R_0). In these evolutions, we utilize gauge conditions (lapse and shift) that are obtained from an exact solution. Hence one of the possible effects is that the gauge

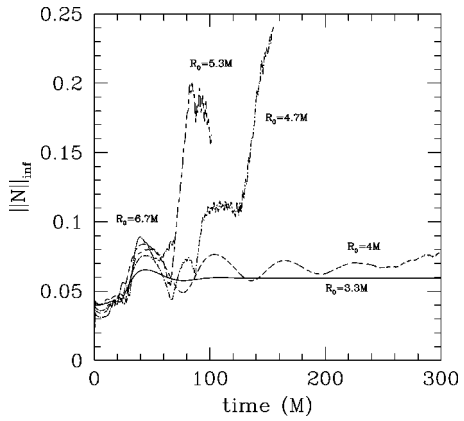

FIG. 2. The l_∞ norm of the normalized Hamiltonian constraint is shown for a series of runs in which the 3D grid spacing was kept fixed and the location of the outer boundary R_0 was moved progressively outwards. Note that for increasing R_0 the maximum runtime decreases. The $R_0=3.33M$ run is stable. This sort of behavior is qualitatively similar to what is seen in spherical symmetry.

behavior may not have the anticipated analytical effect, because of differences arising from numerics during the course of the evolution. Also, for boundary conditions in these 3D evolutions, we use Dirichlet boundary conditions to specify the known solution on the outer boundaries. These may also lead to reflections that perturb the system and add complications to treatment of such questions as to whether the system is well posed.

In preliminary numerical evolutions of single black holes in spherical symmetry, we found similarly stable or unstable evolutions based on the location of the outer boundary. In addition we found that improvement of resolution seemed to improve the maximum runtimes of the unstable runs. This is consistent with results due to Gundlach and Walker [16] who evolved a Schwarzschild black hole using the same choice of lapse and shift as us (ingoing-Eddington-Finkelstein coordinates) but with a different formulation and differencing of the $3+1$ equations.

In a fully 3D evolution, often the task of separating out the source of unbounded growths can be difficult, and just carrying out a process of elimination may be time consuming due to the resource requirements of 3D simulations. This prompted us to carry out a 1D study which we report here that hopefully will help to understand the observed behavior in 3D simulations. We address first some of the questions raised from a numerical point of view and then from an analytical point of view. We use, as closely as possible, the same numerical techniques, boundary conditions, gauge, discretizations, and initial data used in the 3D case. We focus on qualitative similarities between the 3D and 1D time evolutions of Schwarzschild black holes and investigate methods allowing long-term evolutions.

Section II briefly reviews the ADM formalism we use and introduces the spacetime under consideration, namely that of a single black hole. Sec. III presents a numerical study of the 1D situation as compared to that in 3D. Section IV contains a perturbative study of the 1D problem which shows how gauge and constraint violating modes can be generated, modes that could harm the numerical evolution of the full system. We can see that the results of this analysis are consistent with those from the numerical study in that we show how a simple gauge choice eliminates the unstable coupled constraint violating gauge modes. We conclude with a brief discussion on the implications of this work on 3D simulations using not only the ADM approach but also other formulations. Applications of these ideas to the much more difficult 3D case are underway. Preliminary 3D results are consistent with the 1D findings presented in this work.

II. THE ADM SYSTEM

Our study is based on the ''standard'' ADM formulation of the Einstein equations [1]. This $\dot{g}$-$\dot{K}$ system of equations reads

$$(\partial_t-\mathcal{L}_\beta)g_{ij}=-2\alpha K_{ij}, \tag{2.1}$$

$$(\partial_t-\mathcal{L}_\beta)K_{ij}=-\nabla_i\nabla_j\alpha+\alpha(R_{ij}+KK_{ij}-2K_{im}K^m_j), \tag{2.2}$$

with $\mathcal{L}_\beta$ the Lie derivative with respect to the shift vector β^i, α the lapse function, ∇_i and R_{ij}, respectively, the covariant derivative, and the Ricci tensor associated with the spatial metric g_{ij} (with inverse g^{ij}), and $K=g^{ij}K_{ij}$. Additionally, the following equations represent constraints on the field variables, known, respectively, as the Hamiltonian and momentum constraints:

$$R+K^2-K_{ij}K^{ij}=0, \tag{2.3}$$

$$\nabla_j(K^{ij}-g^{ij}K)=0. \tag{2.4}$$

This set of 16 equations, Eqs. (2.1)–(2.4), naturally defines an initial value problem. Initial data satisfying the constraints (2.3) and (2.4) are given at some hypersurface. Then the field variables are evolved to the future by means of the evolution equations (2.1) and (2.2). Notice that, in principle, there is no need to enforce the constraints during the evolution as they *should* be preserved [1] in a consistent numerical implementation; however, one might freely add them to the evolution equations in order to preserve stability or to numerically preserve satisfying the constraints. Our basic evolution schemes are *free* evolutions which do not enforce these constraints.

Several studies exist in the literature about stability of linear waves, not only for the ADM system but also for newer systems [9,18,19]. Unfortunately, results obtained in these studies are not readily applicable in cases which are not approximately Minkowskian. Here we are specifically interested in analyzing the behavior of the ADM system when modeling a black hole spacetime in the spherically symmetric 1D case, and we study a single black hole expressed in terms of ingoing Eddington-Finkelstein coordinates. This choice is motivated by the fact that, in these coordinates, surfaces of constant coordinate time ''penetrate'' the event horizon. The essence of black hole excision is the removal of the singularity while preserving the integrity of the spacetime accessible to observers outside the black hole. As origi-

nally suggested by Unruh [20]), this is possible only if the excised region is fully contained within the event horizon, thus the need to have access to the interior of the black hole.

The line element of the spacetime of a single black hole expressed in ingoing Eddington Finkelstein, spherical coordinates reads

$$ds^2 = -\left(1-\frac{2M}{r}\right)dt^2 + \frac{4M}{r}dtdr + \left(1+\frac{2M}{r}\right)dr^2 + r^2 d\Omega^2, \tag{2.5}$$

where $d\Omega^2 = d\theta^2 + \sin^2\theta d\phi^2$. Given that in this case the spacetime ADM metric is of the form

$$g_{\mu\nu} = \begin{pmatrix} -\alpha^2 + g_{rr}\beta^r\beta^r & g_{rr}\beta^r & 0 & 0 \\ g_{rr}\beta^r & g_{rr} & 0 & 0 \\ 0 & 0 & g_{\theta\theta} & 0 \\ 0 & 0 & 0 & g_{\theta\theta}\sin^2\theta \end{pmatrix}, \tag{2.6}$$

Eq. (2.5) implies that

$$\alpha = \left(1+\frac{2M}{r}\right)^{-1/2},$$

$$\beta^r = \left(\frac{2M}{r}\right)\alpha^2,$$

$$g_{rr} = \alpha^{-2},$$

$$g_{\theta\theta} = r^2 = \frac{g_{\phi\phi}}{\sin^2\theta},$$

$$K_{rr} = -\frac{2M}{r^3}(r+M)\alpha,$$

$$K_{\theta\theta} = 2M\alpha = \frac{K_{\phi\phi}}{\sin^2\theta},$$

where the extrinsic curvature components are obtained from the $\dot{g}$ Eq. (2.1).

III. NUMERICAL ANALYSIS

Our numerical analysis of the onset of instabilities was carried using two second order accurate spherically symmetric codes. One of them solves the full nonlinear set of Einstein equations. The other code solves the linearized version of these equations. Both 1D codes closely resemble the full nonlinear 3D code written by the Binary Black Hole Grand Challenge Alliance [21] and its revision, the AGAVE code [22]. Hence, the results obtained with these 1D codes can hopefully be applied to the 3D model. As with the 3D code, the singularity is excised from the computational domain, and causal differencing [21] is used to discretize the equations. Note that, due to the causal properties of the spacetime, if the inner boundary is placed inside the horizon, no inner boundary data are needed; the excising boundary becomes the analog of an outflow boundary for supersonic fluids. *Outer boundary* data are provided by *blending* [23] the numerical solution to the analytic solution on a region of size M. For the linear evolutions, this corresponds to blending to vanishing perturbations. In all cases, the simulations correspond to evolutions of a black hole of mass M, the inner boundary is placed at $r=lM$ and the outer boundary is placed at $r=nM$ (with $l,n \in N$). We studied the stability of the evolution and its dependence on l and n.

Throughout the present work we adopt a pragmatic definition of stability. In rigor, a numerical implementation is called stable if the solution u at time T satisfies [24]

$$|u(t=T)| \leqslant e^{aT}|u(t=0)|, \tag{3.1}$$

for some constant $a \geqslant 0$ independent of the data. However, in numerical simulations of black hole spacetimes, it is expected that the system at late times will approach a stationary spacetime, and in an appropriate gauge, the solution is not expected to have an exponential form. In the following we will heuristically call a solution *stable* if it does not display an exponential growth to at least $t=500M$ (independent of resolution). This length of time is expected to be enough for accurate simulation of astrophysically relevant systems containing black holes.

A. Linear spherical code results

Several tests were performed with the the linear code. The tests consisted of giving high frequency initial data with amplitude of order Δr^2 for the δg_{rr} as

$$\delta g_{rr} = \mu \sin(\omega r)\left(1-\frac{r}{R_a}\right)^4\left(1-\frac{r}{R_b}\right)^4 \Delta r^2, \tag{3.2}$$

if $r \in [R_a, R_b]$ and $\delta g_{rr}=0$ otherwise (with μ a free parameter and $\omega = \pi/\Delta r$).

Our results can be summarized as follows

Test I: Free evolution. Notably, stable evolutions were obtained for $l=1, n \leqslant 6$ (with discretizations as coarse as $\Delta r = M/8$). However, for $l=1, n>6$, the evolution apparently proceeds stably for about $400M$ but then an instability develops at the inner boundary that crashes the evolution even with discretizations of order $\Delta r = M/384$. To analyze whether these instabilities arise from the numerical or analytical level we run the code using six different resolutions $\Delta r = M/(2^s 3)$ $(s=2\cdots 7)$ and evolved to $t=520M$ for $n=9$. We then analyzed the convergence of $\Pi \equiv \partial_t \delta g_{rr}/\delta g_{rr}$ at the final time and also obtained from each evolution the exponent μ of the growth from plotting $\ln(\|g_{rr}\|)$ vs $\ln\Delta r$. In both cases we observed convergence to an exponential growth of the form $e^{\mu_o t}$ (unstable in our usage). In particular, we observed that $\mu_o \to 0.00958$. These tests clearly suggest that *these modes arise from the continuum arena*. The coefficient of the exponential is also found to vary with the domain, suggesting that is a boundary driven mode.

Test II: Area locked evolution I. We analytically set the perturbation of $g_{\theta\theta}$ to zero. In light of the results obtained in Sec. IV below, by controlling this variable, the secular

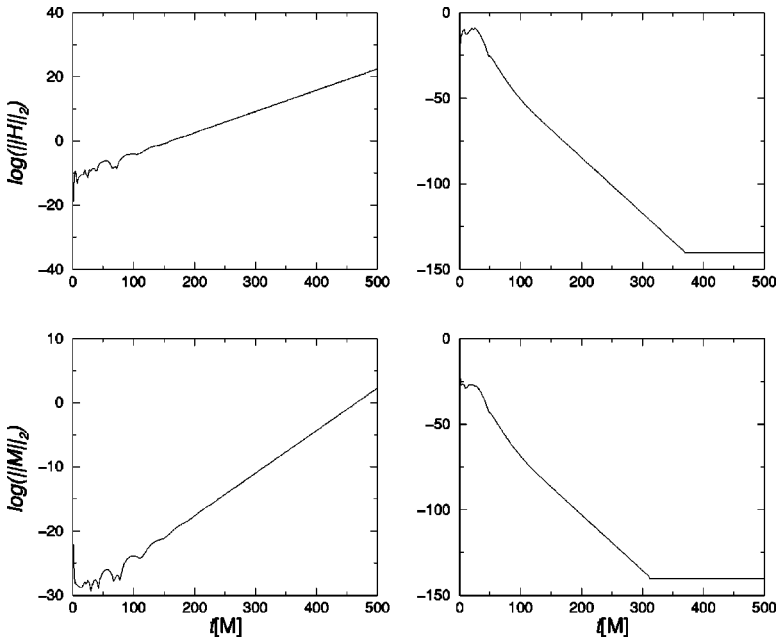

FIG. 3. Linear case: Comparison of runs with and without the locking technique for the linear case (with $\Delta r = M/8$ and $\delta\alpha = \delta\beta^r = 0$). The left column illustrates the (logarithm of the) L_2 norm of the Hamiltonian (H) and momentum (M) constraints for the case without locking. The right column corresponds to the case where locking was used. Stable evolutions were obtained in the latter case.

modes should be removed from the evolution. In this case, test I was repeated under this condition and stable evolutions were obtained regardless of the value of n with discretizations of size $\Delta r = M/8$ and finer.

Test III: Area locked evolution II. Since the area locking technique that will be implemented in the full code involves redefining β^r numerically (see Sec. III B), it is expected that its value will have a Δr^2 error. To check that indeed stability is still achieved despite this error, we introduced a perturbation of $\delta\beta^r$ of the form

$$\delta\beta^r = \nu\left(1-\frac{t}{t_f}\right)^2 \sin(\omega r)\left(1-\frac{r}{R_a}\right)^4\left(1-\frac{r}{R_b}\right)^4 \Delta r^2, \tag{3.3}$$

if $t \leqslant t_f$ and $r \in [R_a, R_b]$ (and 0 otherwise). We chose $t_f = 20M$ and the cases studied in test II were repeated checking that still the evolution proceeded stably.

Test IV: Annulus problem. We chose $l = 10, n = 15$ and fixed the values at the inner and outer boundaries Again, it was found that simulations still required area locking in order to obtain stable evolutions (as the linear analysis of Sec. IV indicates).

Figures 3 and 4 illustrate what happens with and without the locking technique. The plots compare the (logarithm of the) L_2 norm of δg_{rr}, δK_{rr}, the Hamiltonian and the momentum constraints for the case without $\delta g_{\theta\theta}$ locking to the case with $\delta g_{\theta\theta} = 0$. Clearly, unstable evolutions are obtained when $\delta g_{\theta\theta}$ is not under control but locking this variable leads to stable evolutions.

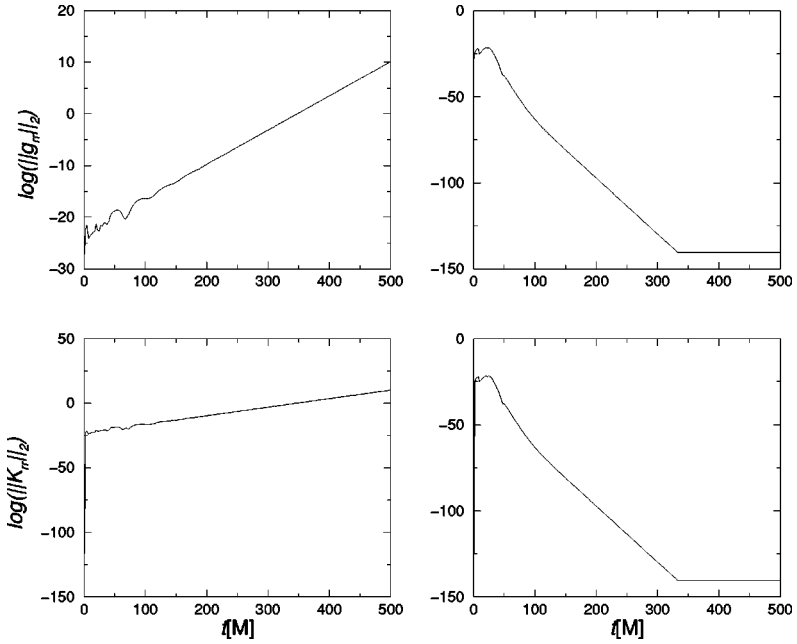

FIG. 4. Linear case: Comparison of runs with and without the locking technique for the linear case (with $\Delta r = M/8$ and $\delta\alpha = \delta\beta^r = 0$). The left column illustrates the (logarithm of the) L_2 norm of δg_{rr} and δK_{rr} for the case without locking. The right column corresponds to the case where locking was used. Stable evolutions were obtained in the latter case.

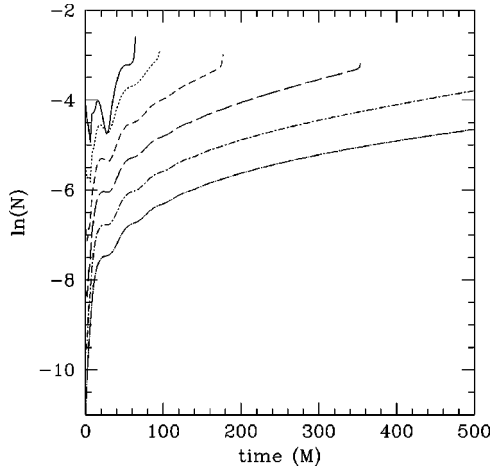

FIG. 5. The l_2 norm of the normalized Hamiltonian constraint as a function of time for a series of resolutions: $\Delta r = M/(3\times 2^s)$ where $s=0,1,2,3,4,5$ from left to right corresponding to the full nonlinear case without area locking and domain $[M,11M]$.

B. Full nonlinear spherical code results

We studied two important and distinct cases. (A) the ''inhole'' case (where $l \leqslant 2 < n$) and (B) the ''annulus problem'' (where $2 < l < n$). In case (A) inner boundary data are not given as they are not needed for the evolution (because of the causal properties inside the horizon) and only outer boundary data are provided. In case (B) boundary data are needed both at the inner and outer boundary. The boundary data, where needed, were given by *blending* the numerically obtained solution to the analytical one. Tests performed with this code fully agree with those of the previous section, albeit instabilities in this case are ''more violent'' than in the linear case as modes couple and instabilities manifest themselves earlier than in the linear case.

Tests performed with this code can be summarized as follows,

Test I: Free evolution. Stable numerical evolutions were obtained when $l=1, n \leqslant 6$ and $\Delta r \leqslant M/8$. Unstable evolutions are found for the case $n>6$ as well as for the annulus problem. Again, an instability develops at the inner boundary which grows exponentially. In these cases, refining the grid produced ''longer'' evolutions (meaning the exponential growth caused the code to crash at a later t) but still unstable ones. To analyze the source of this exponential growth we ran a series of runs with $l=1$ and $n=9$ with resolutions $\delta r = M/(3\times 2^s)$ where $s=1,2,3,4,5,6$. In order to ensure that we have a fixed strength perturbation for all resolutions we introduced the following transformation in r:

$$r \to r(1 + A e^{-(r-r_0)^2/\Delta^2}), \tag{3.4}$$

and recomputed the initial data. With this data and an amplitude of $A=0.01$, width of $\Delta=1$ and pulse location of $r_0 = 5M$ we carried out the series of runs. Figure 5 shows the l_2 norm of the normalized Hamiltonian constraint as a function of time. We find that the constraints converge but exhibit an exponential growth with progressively longer runs with resolution. The violation of the constraints is an indication that we do not have a ''pure'' gauge mode and that constraint violating modes are indeed present in the data which can be generated at the outer boundary and manifest themselves as long-wavelength modes in the time-evolution.

Test II-III: Area locked evolution I-II. In light of the results obtained in Sec. III A and those from Sec. IV below, it is clear that controlling the behavior of $g_{\theta\theta}$ might improve the overall evolution. Since we are dealing with the full nonlinear case, there is no clean distinction between the two cases presented in Sec. III A since, as we shall explain below, there will always be an, at best, inherent second order error in the definition of β^r to achieve the locking of $g_{\theta\theta}$. We employ a version of the so-called ''area locking'' technique in the following way [25]. Analytically, one expects

$$0 = \partial_t g_{\theta\theta} = \beta^r \partial_r g_{\theta\theta} - 2\alpha K_{\theta\theta}. \tag{3.5}$$

Numerically, on the other hand, this equation will only be approximately satisfied, which could then excite the modes discussed in Sec. IV. Thus, one can introduce a modified gauge ($\beta^r \to \beta^r + \delta\beta^r$) that satisfies Eq. (3.5); i.e., $\delta\beta^r$ is such that

$$\delta\beta^r = \frac{\partial_t g_{\theta\theta}}{\partial_r g_{\theta\theta}}. \tag{3.6}$$

In our numerical implementation, we proceed as follows. First, at level n integrate the evolution equations as usual and obtain $g^{n+1}_{\theta\theta}$ Then, evaluate Eq. (3.6) and redefine β^r. Finally, retake the step. This implementation, although twice as expensive as the usual integration, manages to ''lock'' the evolution of $g_{\theta\theta}$. Its advantages are corroborated by the stable evolutions obtained for both the annulus and the ''inhole'' problems with discretizations of size $\Delta r = M/8$ or finer which cannot be obtained otherwise. As an illustration of this behavior Figs. 6 and 7 show the (logarithm of the) L_2 norm of g_{rr}, K_{rr}, the Hamiltonian and the momentum constraints for the case where $l=1$, $n=9$ with and without the locking technique. As is clearly seen from the graphs, not controlling $g_{\theta\theta}$ leads to unstable evolutions and locking this variable provides stable evolutions. It is also interesting to observe the behavior of the apparent horizon area. As it is shown in Figs. 8 and 9 (for the case without and with area locking respectively), the value of the apparent horizon area increases exponentially when $\delta g_{\theta\theta}$ is not controlled (Fig. 8) while its value monotonically increases at early times but approaches a constant asymptotic value when area locking is applied (Fig. 9). Further, this value converges to the analytic value as the Δr is refined. This ''area locking'' method obviously is only as accurate as the accuracy of the simulation (here Δr^2, so this test correspond to test III of Sec. III A).

Test IV: Annulus Problem. We investigated the case where $l=10, n=15$. Unstable evolutions are found for the case where the ''area locking'' technique is not applied. An instability always develops at the inner boundary which grows exponentially. Again, refining the grid produces ''longer'' evolutions (but the evolutions still crash at early times). On the other hand, using the ''area locking'' technique enables stable evolutions.

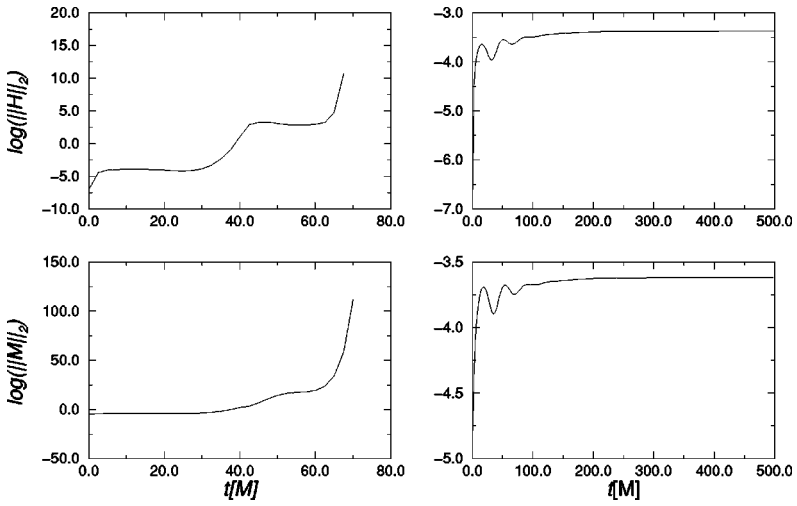

FIG. 6. Nonlinear case: Comparison of runs with and without the locking technique for the fully nonlinear spherical case (with $\Delta r = M/8$ and $\delta\alpha = \delta\beta^r = 0$). The left column illustrates the (logarithm of the) L_2 norm of the Hamiltonian (H) and momentum (M) constraints for the case without locking. The right column corresponds to the case where locking was used. Stable evolutions were obtained in the latter case.

IV. LINEAR PERTURBATION ANALYSIS

The instabilities observed in the full 3D simulations could be of numerical origin or already present at the continuum level. One possible approach to understand the presence of unbound solutions is via a linear perturbation analysis. In order to be useful, a linear perturbation analysis must mimic as closely as possible the conditions present during the numerical simulation. That is, the allowed perturbations in the analysis have to be within the family (e.g., gauge or physical) of perturbations that are triggered by the truncation errors intrinsic to numerical calculations. Specifically, for the spherically symmetric system under consideration, this means that we consider first-order perturbations to the metric (2.5), or, equivalently, Eq. (2.6), of the form

$$g_{\mu\nu} \to g_{\mu\nu} + \delta g_{\mu\nu} \tag{4.1}$$

where

$$-\delta g_{\mu\nu} = \xi^\alpha \partial_\alpha g_{\mu\nu} + g_{\mu\alpha}\partial_\nu \xi^\alpha + g_{\alpha\nu}\partial_\mu \xi^\alpha + \delta M \partial_M g_{\mu\nu} \tag{4.2}$$

with

$$\xi^\alpha = (\delta t, \delta r, 0, 0). \tag{4.3}$$

That is, we are focusing on perturbations generated by gauge or ''coordinate drift'' perturbations of the form

$$r \to r + \delta r, \tag{4.4}$$

$$t \to t + \delta t, \tag{4.5}$$

and, on top of these disturbances, we are also allowing for the possibility of a physical perturbation on the mass of the black hole by considering

$$M \to M + \delta M. \tag{4.6}$$

The perturbations δr, δt, and δM are assumed to be functions of only r and t. We consider δM because during the 3D evolutions of single static black holes, we have evidence that spherical instabilities yield a change in the area of the event horizon, which analytically should be $A = 16\pi M^2$. One infers then that the mass M was shifting during the simulation, see Fig. 1. A similar behavior can be observed in the 1D simulation without $\delta g_{\theta\theta}$ locking, see Fig. 8. In fact, the simulations have no direct method to fix the total mass.

Given the perturbations (4.4)–(4.6), the perturbation to the spacetime metric (2.6) takes the form

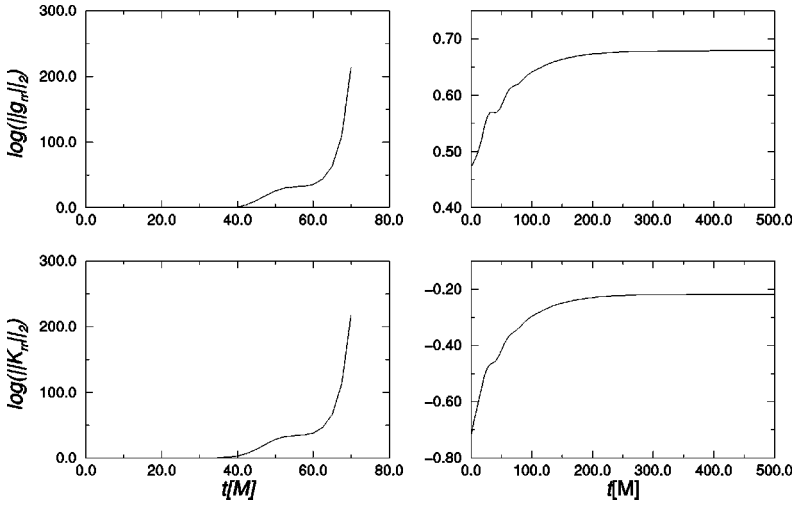

FIG. 7. Nonlinear case: Comparison of runs with and without the locking technique for the fully nonlinear case (with $\Delta r = M/8$ and $\delta\alpha = \delta\beta^r = 0$). The left column illustrates the (logarithm of the) L_2 norm of the g_{rr} and K_{rr} for the case without locking. The right column corresponds to the case where locking was used. Stable evolutions were obtained in the latter case.

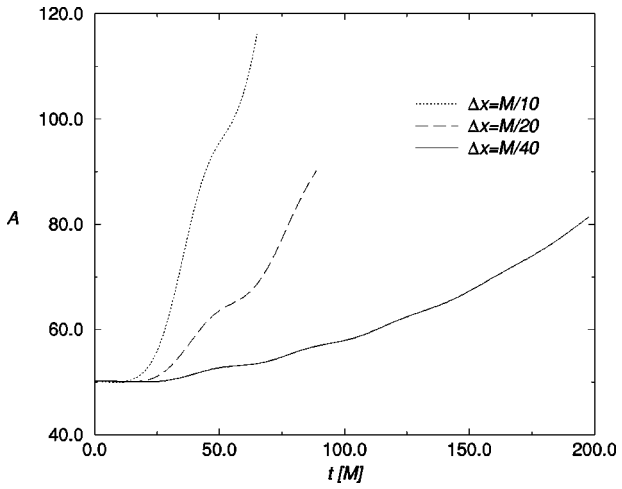

FIG. 8. The area of the apparent horizon for the full nonlinear spherical case without the locking techniques for three different resolutions (10, 20, and 40 points per M). The values obtained are inaccurate and the evolutions eventually crashed (although they last longer as the discretization is refined).

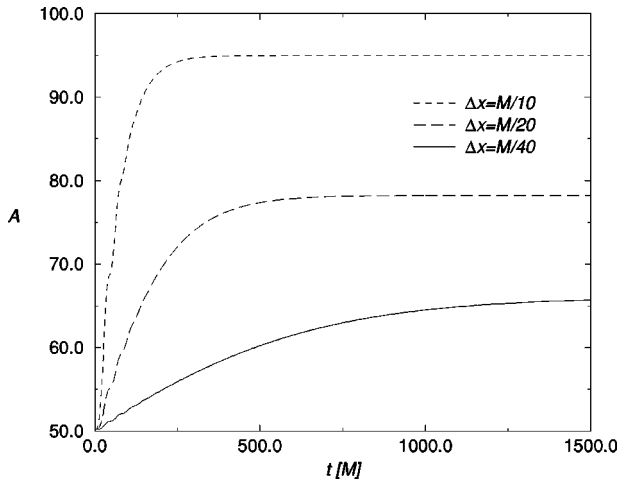

FIG. 9. The area of the apparent horizon for the full nonlinear case with $\delta g_{\theta\theta}$ locked, for three different resolutions (10, 20, and 40 points per M). After some initial transient behavior the value for the area attains a constant value which converges to the expected result as the mesh is refined. Note that these values converge as $O(h)$ because the method used to find the apparent horizon is only first order accurate.

$$\delta g_{\mu\nu} = \begin{pmatrix} \delta(-\alpha^2+g_{rr}\beta^r\beta^r) & \delta(g_{rr}\beta^r) & 0 & 0 \\ \delta(g_{rr}\beta^r) & \delta g_{rr} & 0 & 0 \\ 0 & 0 & \delta g_{\theta\theta} & 0 \\ 0 & 0 & 0 & \delta g_{\theta\theta}\sin^2\theta \end{pmatrix}, \tag{4.7}$$

where

$$\delta(-\alpha^2+g_{rr}\beta^r\beta^r) = \frac{2M}{r}\left(-\frac{\delta M}{M}+\frac{\delta r}{r}-2\partial_t\delta r\right) + 2\left(1-\frac{2M}{r}\right)\partial_t\delta t, \tag{4.8}$$

$$\delta(g_{rr}\beta^r) = \frac{2M}{r}\left(-\frac{\delta M}{M}+\frac{\delta r}{r}-\partial_r\delta r-\partial_t\delta t\right) + \left(1-\frac{2M}{r}\right)\partial_r\delta t-\left(1+\frac{2M}{r}\right)\partial_t\delta r, \tag{4.9}$$

$$\delta g_{rr} = \frac{2M}{r}\left(-\frac{\delta M}{M}+\frac{\delta r}{r}-2\partial_r\delta t\right) - 2\left(1+\frac{2M}{r}\right)\partial_r\delta r, \tag{4.10}$$

$$\delta g_{\theta\theta} = -2r\,\delta r. \tag{4.11}$$

In the 3D numerical simulations of a single black hole in ingoing Eddington-Finkelstein coordinates [26], for which we are interested in investigating the onset of instabilities, the evolution is performed using the analytic (i.e., exact) form of the lapse and shift. Thus, for the spherical perturbation theory we set $\delta\alpha=\delta\beta^r=0$. Imposing vanishing perturbations of the lapse function and shift vector translates into a gauge choice. We focus then on finding out whether this gauge choice admits instabilities at the continuum level when coupled with physical perturbation of the black hole mass. Since α and β^r in ingoing Eddington-Finkelstein coordinates are only functions of M/r, the conditions $\delta\alpha=\delta\beta^r=0$ yield $\delta(M/r)=0$, which in turn becomes

$$\frac{\delta M}{M}=\frac{\delta r}{r}. \tag{4.12}$$

Thus, Eq. (4.12) not only specifies the coupling between gauge and physical perturbations, but it can also be used to eliminate δM from Eqs. (4.8)–(4.10). For instance, substitution of Eq. (4.12) into Eq. (4.10) yields

$$\delta g_{rr} = -\frac{2}{\alpha^2}(\partial_r\delta r+\beta^r\partial_r\delta t). \tag{4.13}$$

Similarly, Eqs. (4.8) and (4.9) yield

$$\partial_o\delta t=0, \tag{4.14}$$

$$\partial_o\delta r=\alpha^4\partial_r\delta t, \tag{4.15}$$

where $\partial_o\equiv(\partial_t-\beta^r\partial_r)$ with β^r the shift vector and α the lapse function in the metric (2.6). Since the operator ∂_o is proportional to the derivative along the normals to the constant t hypersurfaces, Eq. (4.14) states that the perturbation δt is constant along those normals. System (4.15), (4.14) can in fact be re-expressed as

$$\partial_u \delta t = 0, \tag{4.16}$$

$$\partial_u \delta r = \frac{1}{2}\frac{\alpha^4}{(1-\alpha^2)}\partial_v \delta t, \tag{4.17}$$

where $u = t - \rho$ and $v = t + \rho$. The radial coordinate ρ is obtained from $d\rho = dr/\beta^r$, namely,

$$\rho = r\left[1 + \frac{1}{2}\left(\frac{r}{2M}\right)\right]. \tag{4.18}$$

Notice that because of the form of $\rho(r)$, characteristic velocities associated with u and v go to zero as $r \to \infty$. A general solution to the system of Eqs. (4.16) and (4.17) is

$$\delta t = F(v), \tag{4.19}$$

$$\delta r = G(v) - M\partial_v F(v)\left[\frac{t}{M} + \frac{1}{(1-\alpha^2)} + \frac{1}{3(1-\alpha^2)^3}\right]; \tag{4.20}$$

with $F(v)$ and $G(v)$ arbitrary functions of v and, in general, these solutions admit unbounded growing modes. Given these solutions, the metric perturbations $\{\delta g_{rr},\ \delta g_{\theta\theta}\}$ are obtained from Eqs. (4.13) and (4.11), respectively. Since this is not a pure gauge transformation, the perturbations $\{\delta g_{rr},\ \delta g_{\theta\theta}\}$ constructed in this way are consistent with the analytic lapse and shift, but are not in general solutions to the linearized Einstein equations. We proceed by analytically mimicking our computational approach: we demand now that $\{\delta g_{rr},\ \delta g_{\theta\theta}\}$ satisfy the evolution equations and we continue to monitor the constraints.

From Eqs. (A3), (A4), with equations (4.11), (4.13) for the metric perturbation, using the definition of the extrinsic curvature in terms of the metric time derivative, and eliminating time derivatives using Eqs. (4.14), (4.15), the evolutions equations become

$$0 = (r+2M)^2\delta r - r^2(r+2M)\partial_r \delta r + r^3\partial_r \delta t, \tag{4.21}$$

$$\begin{aligned} 0 = &-2(r+2M)^4\delta r + 2r^2(r+2M)(r^2-2M^2)\partial_r \delta r \\ &-2r^4(r+2M)\partial_r \delta t - r^4(r+2M)^2\partial_{rr}\delta r + 2r^5 \\ &\times(r+2M)\partial_{rr}\delta t. \end{aligned} \tag{4.22}$$

By using Eq. (4.21) and its derivative, the r-derivatives of δt can be eliminated from Eq. (4.22) to obtain an equation for δr alone,

$$0 = 2(4M^2 - 3rM - 2r^2)\delta r + 2r^2(2r+3M)\partial_r \delta r - r^4\partial_r^2 \delta r. \tag{4.23}$$

Notice that once Eq. (4.23) is solved for δr, then δt follows from Eq. (4.21) by quadrature. Writing

$$\delta r = r^2 e^{-3M/r} U, \tag{4.24}$$

the equation for U becomes

$$\partial_r^2 U - r^{-4}(2r^2 + 12rM + 17M^2)U = 0. \tag{4.25}$$

Thus the solution to Eq. (4.23) can be expressed, not very informatively, in terms of Whitakker functions [27] as

$$\begin{aligned} \delta r = &C_1 r^3 \mathbf{M}\left(-6\sqrt{17}, \frac{3}{2}, \frac{2M\sqrt{17}}{r}\right) e^{-3M/r} \\ &+ C_2 r^3 \mathbf{W}\left(-6\sqrt{17}, \frac{3}{2}, \frac{2M\sqrt{17}}{r}\right) e^{-3M/r}, \end{aligned} \tag{4.26}$$

where $\mathbf{M}$ and $\mathbf{W}$ denote the Whittaker functions and C_1, C_2 are to be determined from boundary conditions. More informatively, is that the sign of $\partial_r^2 U/U$ in Eq. (4.25) is positive on $(0,\infty)$, and in particular on our computational domain $[lM, nM]$. Thus the graph of U is concave away from the r-axis, and since δr in the computational solution is held to zero at the outer boundary, U does not cross the axis within our computational domain.

Our computational black hole approach excises the inner boundary and sets data only at the outer boundary. Since Eq. (4.25) is a second order equation, both δr and $\partial_r \delta r$ have to be set there. Analytically, setting both to zero at the outer boundary gives the desired solution ($\delta r = 0$ everywhere). However, if δr is set to zero at the outer boundary, the value of δr at the excision region is very sensitive to the value of $\partial_r \delta r$ at the outer boundary. Small computational effects at this boundary can drive large excursions from the desired gauge configuration, as we see in the computational solutions; and the effect is greater for larger domains, consistent with the computational observations. This analysis also shows clearly why gauge fixing $\delta g_{\theta\theta} = -2r\delta r = 0$ solves the instability, since it prevents the large crash-causing δr excursions.

Even with the analysis so far, we have not yet enforced solution of the constraint equation. The Einstein vacuum field equations (including the constraints) are of course satisfied for pure gauge (coordinate) transformations of a vacuum solution. However, by allowing a variation in M, we violate these equations and it is not a surprise that constraint-violating modes can appear. In the context of a numerical simulation, errors in the prescription of initial data can lead to constraint violations.

From Eqs. (A6) and (A7), we have, for the Hamiltonian constraint H and the momentum constraint M^r:

$$H \propto (r+2M)^3\delta r - r^2(r+2M)(r+4M)\partial_r \delta r + 2r^3 M\partial_r \delta t, \tag{4.27}$$

$$M^r \propto 2M^2/r^2(r+2M)\partial_r \delta r + M\partial_r \delta t, \tag{4.28}$$

Clearly, for arbitrary δr and δt the constraints will, in general, be violated. By combining Eqs. (4.27) and (4.28) the requirements that the constraints be satisfied ($H = M^r = 0$) is simply:

$$\partial_r \delta r = \frac{\delta r}{r}, \tag{4.29}$$

with the obvious solution $\delta r \propto r$. Hence, the constraints are satisfied only if

$$\frac{\delta r}{r} = \frac{\delta M}{M} = \text{const.} \tag{4.30}$$

In other words, given our gauge form (specifically α and β^i analytically given as functions of M/r), only scale offsets in r and corresponding offsets in M are allowed. This assures the constancy of the horizon area and the stability of the simulation.

V. DISCUSSION

The results presented in this work show how even small inconsistencies in the choice of coordinate conditions, easily generated by a choice of initial data not in full agreement with the gauge under consideration, can lead to unstable evolutions. This suggests, not surprisingly, that some sort of ''live conditions'' (i.e., gauge conditions that respond to the dynamics of the field) are required for achieving long term evolutions. The fact that these ''gauge-constraint violating modes'' can have unbounded growth is not only harmful for systems such as the ADM one (which does not separate variables into gauge-independent quantities) but also for ''gauge separating'' schemes. These schemes still evolve gauge-dependent quantities and, although these quantities should not affect the gauge-independent ones, the numerical implementation has to either be capable of handling some exponentially growing variables or introduce some special *ad hoc* handling of these terms [28]. Numerical implementations of well posed systems in 1D have also shown the need of having a special treatment of some terms to remove exponentially growing solutions [15].

It is thus interesting to see how a rather simple condition, at least in the spherically symmetric case, can consistently eliminate such growing modes. The success of such a condition highlights the need for deeper studies in the formulation of coordinate (and gauge enforcement) conditions for the generic case. There exists in the literature a few proposals for such generic conditions [25,29,30]. Researchers have started testing those conditions though it is yet unclear whether they hold the key to the general problem. The result demonstrated by the linear continuum analysis, that δr and its derivative at the outer boundary sensitively determine the stability behavior of the solutions, demonstrates that boundary effects, gauge modes, and constraint modes can interact strongly in the behavior of the solution. One could imagine a boundary algorithm which did control the behavior of δr, and had correct convergence properties. Clearly, locking the coordinates so that $\delta r = 0$ throughout the domain as we do is the more robust solution.

The results presented in this paper have a strong bearing on our fully 3D nonlinear evolutions of single black holes. In the 3D evolutions using exact lapse and shift of single Schwarzschild black holes in ingoing Eddington-Finkelstein coordinates we find similar dependence of stability on the outer boundary placement. The computational domain in that scenario is a 3D rectangular grid in which the black hole excision region is embedded. The inner boundary or boundary of excision is left as a causal boundary (as here) and we place Dirichlet conditions at the outer faces or on a spherical or cubical blending shell. This work now focuses our attention on the application of gauge conditions for single black holes in 3D to area locking similar to our 1D results, and points the way to possible issues that we will face in the late stages of binary black hole coalescence. Preliminary 3D work shows improved performance when area locking is carried out. These results are being validated and extended, and will be communicated in the future.

The techniques of this paper can obviously be applied to formulations other than ADM. In particular we have begun a 1D (spherical) study of the ''conformal ADM formulation'' [8,9], where the 3D black hole simulations suggest the existence of similar modes to the 1D and 3D results of the ADM formulation discussed here.

ACKNOWLEDGMENTS

This work was supported by Grant Nos. NSF PHY 9407194 to the University of California, Santa Barbara, NSF PHY 9800722 and NSF PHY 9800725 to the University of Texas at Austin, and NSF 9800970 and NSF 9800973 to the Pennsylvania State University. We thank A. Ashtekar, W. Landry, D. Neilsen, R. Price, and J. Pullin for comments and helpful discussions. We specially thank P. Laguna for extensive discussions and criticisms of the work presented here. L.L. wishes to thank the National University of Cordoba and The Pennsylvania State University where parts of this work were carried out. M.H., L.L. and R.M. thank the Institute for Theoretical Physics, University of California, Santa Barbara where some of this work was carried out.

APPENDIX: LINEARIZED EXPRESSIONS

To first order on the perturbations $\{\delta g_{rr},\ \delta g_{\theta\theta},\ \delta K_{rr},\ \delta K_{\theta\theta}\}$, the Einstein evolution equations (2.1) and (2.2) with $\delta\alpha = \delta\beta^r = 0$ take the form

$$\partial_o \delta g_{rr} = -2\alpha\,\delta K_{rr} + 2\,\delta g_{rr}\partial_r \beta^r, \tag{A1}$$

$$\partial_o \delta g_{\theta\theta} = -2\alpha\,\delta K_{\theta\theta}, \tag{A2}$$

$$\begin{aligned}\partial_o \delta K_{rr} = {} & 2\,\delta K_{rr}\partial_r\beta^r + \delta\Gamma^r_{rr}\partial_r\alpha \\ & + \alpha(\delta R_{rr} + \delta K K_{rr} + K\,\delta K_{rr} - 4g^{rr}K_{rr}\delta K_{rr} \\ & - 2K_{rr}^2\delta g^{rr}),\end{aligned} \tag{A3}$$

$$\begin{aligned}\partial_o \delta K_{\theta\theta} = {} & \delta\Gamma^r_{\theta\theta}\partial_r\alpha + \alpha(\delta R_{\theta\theta} + \delta K K_{\theta\theta} + K\,\delta K_{\theta\theta} \\ & - 4g^{\theta\theta}K_{\theta\theta}\delta K_{\theta\theta} - 2K^2_{\theta\theta}\delta g^{\theta\theta}),\end{aligned} \tag{A4}$$

where

$$\delta\Gamma^r_{rr}=\frac{1}{r+2M}\left(\frac{r}{2}\partial_r\delta g_{rr}+\frac{M}{r+2M}\delta g_{rr}\right),$$

$$\delta\Gamma^r_{\theta\theta}=\frac{r}{r+2M}\left(\frac{r^2}{r+2M}\delta g_{rr}-\frac{1}{2}\partial_r\delta g_{\theta\theta}\right),$$

$$\delta R_{rr}=\frac{1}{r^2}\partial_{rr}\delta g_{\theta\theta}-\frac{2M}{r(r+2M)^2}\delta g_{rr}-\frac{1}{r+2M}\partial_r\delta g_{rr}+2\frac{r^2+3Mr+2M^2}{r^4(r+2M)^2}\delta g_{\theta\theta}-\frac{2r^2+7Mr+6M^2}{r^3(r+2M)^2}\partial_r\delta g_{\theta\theta},$$

$$\delta R_{\theta\theta}=\frac{M}{2(r+2M)^2}\partial_r\delta g_{\theta\theta}-\frac{r^3}{2(r+2M)^2}\partial_r\delta g_{rr}-\frac{r^2(r+4M)}{(r+2M)^3}\delta g_{rr}+\frac{r}{2(r+2M)}\partial_{rr}\delta g_{\theta\theta}. \tag{A5}$$

Similarly, the Hamiltonian and momentum constraints, Eqs. (2.3) and (2.4) respectively, to first order on the perturbations yield:

$$\frac{1}{2M+r}\left[\frac{(8M^3+8M^2r+6Mr^2+r^3)}{r^2(2M+r)^2}\delta g_{rr}-\frac{(4M^2+r^2)}{r^5}\delta g_{\theta\theta}+\left(\frac{r}{2M+r}\right)\partial_r\delta g_{rr}+\frac{(M+r)}{r^2(2M+r)}\partial_r\delta g_{\theta\theta}-\frac{1}{r}\partial_{rr}\delta g_{\theta\theta}+\left(\frac{4M}{2M+r}\right)\sqrt{1+\frac{2M}{r}}\delta K_{rr}+\frac{4M^2}{r^3(2M+r)}\sqrt{1+\frac{2M}{r}}\delta K_{\theta\theta}\right]=0, \tag{A6}$$

$$\frac{M}{r\sqrt{r(r+2M)}}\left[\frac{2(M+r)}{(2M+r)^2}\delta g_{rr}-\frac{2}{r^3}\delta g_{\theta\theta}+\frac{M}{r^2(2M+r)}\partial_r\delta g_{\theta\theta}\right]+\left[\frac{\delta K_{rr}}{2M+r}+\frac{\delta K_{\theta\theta}}{r^3}-\frac{\partial_r\delta K_{\theta\theta}}{r^2}\right]=0, \tag{A7}$$

respectively. The only component of the momentum constraint that is shown is the r direction since the angular components are automatically satisfied to first order in the perturbations.

[1] C. Misner, K. S. Thorne, and J. Wheeler, *Gravitation* (Freeman, San Francisco, 1973).
[2] H. Friedrich, Proc. R. Soc. London **A375**, 169 (1981); **A378**, 401 (1981).
[3] O. Brodbeck, S. Frittelli, P. Huebner, and O. Reula, J. Math. Phys. **40**, 909 (1999).
[4] S. Frittelli and O. Reula, Phys. Rev. Lett. **76**, 4667 (1996).
[5] A. Anderson and J. York, Phys. Rev. Lett. **82**, 4384 (1999).
[6] S. Frittelli and O. Reula, J. Math. Phys. **40**, 5143 (1999).
[7] C. Bona, J. Masso, E. Seidel, and J. Stela, Phys. Rev. D **56**, 3405 (1997).
[8] M. Shibata and T. Nakamura, Phys. Rev. D **52**, 5428 (1995).
[9] T. Baumgarte and S. Shapiro, Phys. Rev. D **59**, 024007 (1999).
[10] M. Alcubierre, B. Brügmann, M. Miller, and W. M. Suen, Phys. Rev. D **60**, 064017 (1999).
[11] M. Scheel and G. Cook, in Proceedings of the ''Miniprogram of Colliding Black Holes: Mathematical Issues in Numerical Relativity,'' Institute for Theoretical Physics, UCSB, 2000.
[12] M. Alcubierre, Ref. [11], Institute for Theoretical Physics, UCSB, 2000.
[13] E. Seidel and W. M. Suen, gr-qc/9210016, 1992.
[14] R. Marsa and M. Choptuik, Phys. Rev. D **54**, 4929 (1996).
[15] M. Scheel, T. Baumgarte, G. Cook, S. Shapiro, and S. Teukolsky, Phys. Rev. D **58**, 044020 (1998).
[16] C. Gundlach and P. Walker, Class. Quantum Grav. **16**, 991 (1999).
[17] S. Hawking, in *Black Holes*, edited by C. De Witt and B. De Witt (Gordon & Breach, New York, 1972).
[18] M. Alcubierre, G. Allen, B. Brügmann, E. Seidel, and W. M. Suen, gr-qc/9908079, 1999.
[19] S. Frittelli, R. Gomez, O. Reula, and P. Huebner (private communication).
[20] J. Thornburg, Class. Quantum Grav. **4**, 1119 (1987).
[21] M. Huq and R. Matzner (unpublished).
[22] http://www.astro.psu.edu/users/nr/Agave/
[23] L. Rezzolla, A. Abrahams, R. Matzner, M. Rupright, and S. Shapiro, Phys. Rev. D **59**, 064001 (1999).
[24] B. Gustaffson, H. Kreiss and J. Oliger, *Time Dependent Problems and Difference Methods* (Wiley, New York, 1995).
[25] C. Gundlach and D. Garfinkle, Class. Quantum Grav. **16**, 4111 (1999).
[26] The Binary Black Hole Grande Challenge Alliance, Phys. Rev. Lett. **80**, 2512 (1998).
[27] E. T. Whitakker, *A Treatise on the Analytical Dynamics of Particles and Rigid Bodies* (Cambridge University Press, Cambridge, England, 1937).
[28] A. Arbona, C. Bona, J. Masso, and J. Stela, Phys. Rev. D **60**, 104014 (1999).
[29] L. L. Smarr and J. W. York, Phys. Rev. D **17**, 2529 (1978).
[30] P. R. Brady, J. D. Creighton, and K. S. Thorne, Phys. Rev. D **58**, 061501 (1998).